J Appl Electrochem (2011) 41:721–730
DOI 10.1007/s10800-011-0286-z

ORIGINAL PAPER

Buffered electrochemical polishing of niobium

Gianluigi Ciovati · Hui Tian · Sean G. Corcoran

Received: 5 April 2010 / Accepted: 10 March 2011 / Published online: 31 March 2011

Abstract The standard preparation of superconducting radio-frequency (SRF) cavities made of pure niobium include the removal of a "damaged" surface layer, by buffered chemical polishing (BCP) or electropolishing (EP), after the cavities are formed. The performance of the cavities is characterized by a sharp degradation of the quality factor at high surface magnetic field, a phenomenon referred to as "Q-drop". In some cases, the Q-drop can be significantly reduced by a low-temperature ($\sim$120 °C) "in situ" baking of the cavity. As part of the effort to understand this phenomenon, the effect of introducing a polarization potential during BCP, creating a process which is between the standard BCP and EP, was investigated. The focus of this contribution is on the characterization of this novel electrochemical process by measuring polarization curves, etching rates, surface finish, and electrochemical impedance. In particular, it is shown that the anodic potential of Nb during BCP has a plateau region in the polarization curve and the impedance diagrams on the plateau can be described with a "surface charge" model found in the literature. By applying an anodic potential to Nb, a lower etching rate and better the surface finish than by standard BCP process have been obtained.

Keywords Niobium · Electrodes · Electropolishing · Etching

G. Ciovati (✉) · H. Tian
Thomas Jefferson National Accelerator Facility,
12000 Jefferson Avenue, Newport News, VA 23606, USA
e-mail: gciovati@jlab.org

S. G. Corcoran
Materials Science & Engineering Department, Virginia Tech,
460 Turner Street, Blacksburg, VA 24060, USA

1 Introduction

Niobium superconducting radio-frequency (SRF) cavities are widely used in modern particle accelerators, because of higher operating efficiency than normal-conducting cavities made of copper. Since the superconducting RF current flows in a surface layer about 40 nm deep, a set of preparation techniques have been developed over the years to assure good superconducting properties of the surface layer [1]. In particular, the removal of a "damaged" layer of about 200 μm, resulting from the mechanical forming of the cavity, and a "contaminated" layer of about 20–50 μm, resulting from the gettering of impurities by the Nb surface during high-temperature heat treatments, is achieved by either chemical etching or electropolishing. These chemical treatments result in a typical RMS surface roughness of about 1.6 ± 0.42 μm and about 0.34 ± 0.11 μm, over a 50 μm × 50 μm scan area, for buffered chemical polishing (BCP) and electropolishing (EP), respectively [2, 3]. A figure of merit of SRF cavities is the so-called quality factor which is a measure of the efficiency of the cavity in storing electromagnetic energy and is inversely proportional to the surface resistance of the cavity walls. The performance of SRF Nb cavities treated by BCP or EP is characterized by a sharp degradation of the quality factor above a surface magnetic field of about 90 mT; a phenomenon commonly referred to as "Q-drop". It was found that a low-temperature baking ($\sim$120 °C, 12–48 h) of the cavities in ultra-high vacuum produced a significant improvement of the Q-drop in polycrystalline, fine-grain (ASTM 5) Nb cavities treated by EP but not BCP [4]. Therefore, EP has emerged as the surface treatment of choice to produce cavities which can reach surface magnetic fields close to the theoretical limit of Nb [5]. However, the EP treatment is more expensive and time consuming than BCP. It should also be

mentioned that recent research on cavities built from single-crystal and large-grain Nb and treated by BCP showed a smooth surface finish and performance comparable to electropolished cavities [6].

Several models have been proposed over the past 10 years to explain the Q-drop and the baking effect but a comprehensive explanation of the experimental data is yet to be found. In particular, one model relates the Q-drop to a high density of localized states in the non-stoichiometric niobium pentoxide Nb_2O_{5-y} (for example due to oxygen vacancies) which is readily formed on the niobium surface after exposing the pure metal to air or water [7]. Differences in the stoichiometry and defect density between the oxide formed on an electropolished surface and the one formed on a chemically etched surface could account for the different cavity performance after baking [7].

During the standard BCP process, a mixture of hydrofluoric (49%), nitric (70%), and phosphoric acid (85%) by volume ratio of 1:1:1 or 1:1:2 is used with a temperature range of 10–25 °C. Niobium is oxidized by the nitric acid and the oxide layer is removed by the hydrofluoric acid, resulting in etching of the surface. This reaction is highly exothermic and the phosphoric acid is used as a buffer to reduce the etching rate. During the standard EP of niobium, anodic dissolution of the metal is obtained in a 1:9 volume ratio mixture of hydrofluoric (49%) and sulfuric acid (96%) at a temperature of 30–40 °C with a current density of 30–100 mA cm^{-2}. Both BCP and EP processes have been used for the polishing of the Nb surface of SRF cavities for more than 20 years.

The oxidation of niobium in the ambient atmosphere is a field assisted process (Cabrera-Mott model), where oxygen ions are attracted to the metal by a negative contact potential (Mott potential $V_M \sim -0.6$ V), yielding the Nb_2O_5 growth. In the early stage of growth, the oxide growth rate is limited by the diffusion of ions aided by the Mott potential, while in the later stage it is limited by the tunneling of electrons through the oxide aided by a positive ionic diffusion potential ($V_D \sim 0.17$ V) limiting the Nb_2O_5 thickness to about 2–3 nm [8]. The oxide layer formed on the Nb surface is generally "microcrystalline amorphous," non-stoichiometric Nb_2O_{5-y}, $y < 0.5$. Oxide defects include extended defects, such as crystallographic shear planes, and localized defects, such as oxygen vacancies. The density of defects is typically higher by oxidation in the presence of water ("wet" oxide) than in the presence of oxygen gas ("dry" oxide) [8].

In fluid electrolytes, the application of a small potential to the Nb cavity during BCP may enforce (anodic potential) or slow (cathodic potential) the oxidation process. Preliminary results on the performance of a Nb cavity after application of this process are reported elsewhere [9] and no significant difference from the performance of a cavity treated by standard BCP was observed. In those experiments, a low voltage (<1 V, anodic or cathodic) and low current density (1–3 mA cm^{-2}) was applied between the cavity and a Nb rod coaxial to the cavity, used as counter electrode. The surface area ratio of the cavity to the Nb rod was 13:1.

In order to gain a better understanding of the electrochemical process occurring during the polarized BCP, we measured the anodic and cathodic polarization curves of Nb in the 1:1:2 mixture, the resistivity of the electrolyte, the etching rates, and surface finish for anodic and cathodic polarizations. These measurements have been done on both flat and cylindrical electrodes. In addition, electrochemical impedance spectroscopy (EIS) with rotating disk electrode (RDE) technique has been used to characterize the electrochemical process. Impedance data in the plateau region of the polarization curve are discussed with reference to the surface charge model for the formation/dissolution of the barrier oxide film [10].

2 Experimental

In the flat electrode configuration, two high purity polycrystalline Nb (99.9999%, Teledyne Wah-Chang) samples with dimensions of 16 mm × 22 mm × 3 mm are embedded into Teflon sample holders, providing an exposed surface area of 2.6 cm^2 for the cathode and 1.4 cm^2 for the anode. The separation between electrodes was 98 mm. In the cylindrical electrode configuration, the anode consists of a high purity polycrystalline Nb cylinder (99.9999%, Teledyne Wah-Chang) of 70 mm inner diameter, 3 mm thick, 100 mm height, sealed at one end with a Teflon disk. The cathode consists of a lower purity Nb tube (99.99%, Teledyne Wah-Chang) of 29 mm outer diameter, 2 mm thick, 180 mm long, coaxial with the other electrode. The cylindrical electrodes configuration mimics the setup for polishing Nb cavities, while the flat electrodes configuration allows for easier analysis of the surface finish. Because most common metals will be etched by the BCP mixture, Nb was chosen as counter electrode in order to avoid possible contamination of the Nb working electrode by the counter electrode material; a situation which is unacceptable for the treatment of Nb cavities. The reference electrode was a saturated mercury mercurous-sulfate electrode (MSE) placed about 10 mm from the sample and about 5 mm from the cylinder, in the flat and cylindrical electrode configurations, respectively. To protect the reference electrode from HF contamination, the electrode was placed in a PTFE electrode bridge tube with a Vycor frit. The electrode bridge tube was filled with 1 M H_2SO_4 as the conductive electrolyte. The electrolytes were prepared from reagent grade 49% hydrofluoric (48.8–49.2%, J. T. Baker), 85% phosphoric (85–87%, J. T. Baker), and

Table 1 Estimated composition of the acid mixtures used for BCP and EP

	Reagent conc. (Mass%)	BCP 1:1:2 (mol L^{-1})	EP (mol L^{-1})
HF	49	7.23	2.89
HNO_3	70	3.98	–
H_3PO_4	85	7.4	–
H_2SO_4	96	–	16.2
H_2O	100	21.02	7.02

70% nitric acid (69–70%, J. T. Baker). The composition of the acid mixture used for these experiments are given in Table 1, along with the composition of the electrolyte used for the EP process, as a comparison.

In the flat electrode configuration, the Teflon block holding the samples is immersed in a large container filled with the electrolyte and the temperature is adjusted with a water bath. In the cylindrical electrode configuration, the electrolyte is contained in the space between the two electrodes and the temperature is adjusted with a water bath. It is worthwhile to notice that in the cylindrical electrode configuration a much smaller volume of acid mixture is used for a much larger Nb surface, compared to the flat electrode configuration. The electrolyte was kept in static condition (no agitation) during all measurements.

A Sorensen DCS 33-33E power supply was used to apply a voltage, V_{ps}, between the Nb anode and cathode electrodes. The anode and cathode potentials were measured relative to the reference electrode, placed near the anode or cathode, respectively, using a Keithley 6517A electrometer. For currents below 3 A, a HP 3478A multimeter was used, while the power supply readout was used for higher currents. The data acquisition was supported by a customized LabView program. The value of the current is the average of 10 consecutive measurements.

Impedance measurements were performed with a Gamry Instruments G300 potentiostat controlled with a commercial software package (Gamry Instrument Framework). Impedance measurements were performed at a constant applied dc potential added to a small ac potential (10 mV rms amplitude) in the frequency range from 200 kHz to 1.6 Hz. A Gamry RDE710 was used for the rotating electrode setup. For EIS measurements, a high purity polycrystalline Nb disk electrode (19.63 mm^2 surface area) was inserted in a Teflon holder. The Nb disk was mechanically polished up to 4000 grit emery paper, cleaned in isopropanol with ultrasonic agitation, and rinsed with distilled water and air dried. A high purity Al wire was used as the counter electrode.

All the experiments mentioned above have been performed under a chemical flow hood for safety reasons.

3 Results

3.1 Polarization behavior

Figure 1 shows the typical polarization behavior for the Nb disk electrode. Similar polarization curves were obtained for the flat and cylindrical electrode configurations. The open circuit potential of the Nb in $HF:HNO_3:H_3PO_4$ = 1:1:2 mixture at 20 °C, relative to the MSE reference electrode is about -0.150 ± 0.005 V (+0.490 V versus SHE). Current oscillations were observed at positive potentials in the range 0.3–1.3 V versus MSE followed by a current plateau at higher anodic potential. The current density in the plateau region increases approximately linearly as a function of the temperature of the acid bath, as shown in Fig. 2. Each data point in Fig. 2 is the average of two measurements and the value of the current density, J, is at a potential of 2.4 V versus MSE.

The resistivity of the electrolyte was approximated from the difference in anode potential measured relative to two different reference electrode locations (one near the anode and one near the cathode), as a function of the current flow, for current density up to ~ 100 mA cm^{-2}. The value obtained for both flat and cylindrical electrodes configurations was about 35 mΩ cm at bath temperatures of 10–23 °C.

3.2 Surface topography

Optical images of the flat anode and cathode surfaces after processing were taken with a Hirox KH-3000VD digital optical microscope. The flat electrodes were polished in the current plateau region ($V_{ps} = 3$ V, $E_{anode} = 2.2$ V vs. MSE, $J = 110$ mA cm^{-2}, $T_{bath} = 10$ °C) for about 1 h,

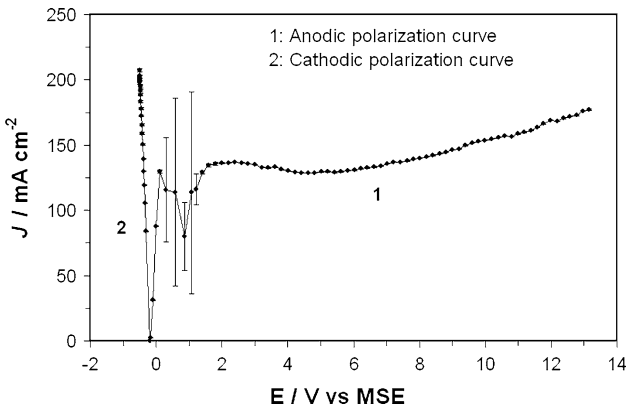

Fig. 1 Typical polarization behavior for Nb disk electrode with Al wire as counter electrode in HF (49%):HNO_3 (70%):H_3PO_4 (85%) = 1:1:2 (volume ratio) at 13 ± 1 °C. The voltage between the anode and cathode was controlled in a two electrode configuration. The potential of the electrodes was measured using a saturated mercury mercurous sulfate reference electrode (MSE)

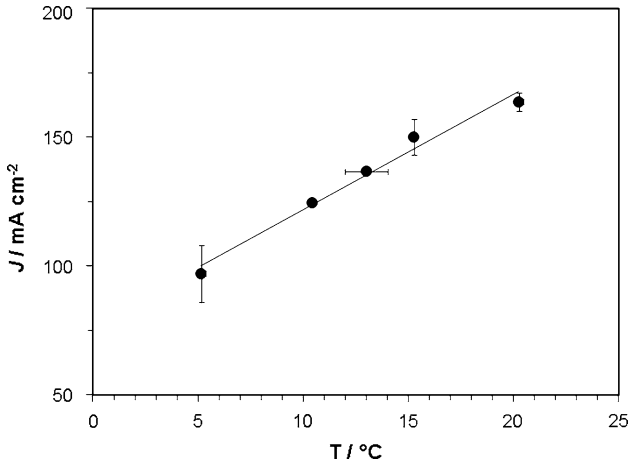

Fig. 2 Temperature dependence of the current density measured at 2.4 V versus MSE. The *solid line* is a linear fit of the data

using the 1:1:2 mixture as the electrolyte. Optical microscopy of the anode (Fig. 3a) shows a smooth surface, somewhat similar to EP, while the cathode finish resembles that of standard BCP (Fig. 3b). Nevertheless, some regions of the anode showed several pits (Fig. 3c). The density of pits, their average radius, and depth were 131 pits cm^{-2}, 40 ± 6 μm (average of 34 pits), and 21 ± 7 μm (average of 15 pits), respectively. A high purity Nb sample was etched in the same 1:1:2 mixture without any potential applied and the surface finish is shown in Fig. 3d for comparison. No pits were observed on either the cathode or on the buffered chemical polished sample. The material removal was measured by weight loss and with a micrometer and the resulting etching rates were 1.15 μm min^{-1}, 0.67 μm min^{-1}, and 1.03 μm min^{-1} for the cathode, anode, and chemically polished Nb samples, respectively. The RMS value of the surface roughness of the anode was measured over an area 50 μm × 50 μm with an atomic force microscope (Digital Instrument Dimension Nanoscope IV operated in the Tapping Mode with an ultrasharp silicon tip of a diameter of 10 nm). The average value of the RMS roughness for eight different locations on the anode is 113 ± 41 nm, comparable to values measured on electropolished surfaces. The average value of the peak-to-valley height is 759 ± 151 nm. The average value of the RMS roughness prior to chemical polishing was 390 ± 50 nm. Figure 4 shows a plot of the surface topography over a 50 μm × 50 μm area measured by atomic force microscopy (AFM).

3.3 Impedance experiments

Impedance measurements were performed using a freshly prepared HF:HNO_3:H_3PO_4 mixture (1:1:2 by volume) as a function of applied potential (E = 2–7 V relative to MSE), with no agitation, and at a fixed potential (E = 4 V relative to MSE) but different speed (20–100 rpm) of the RDE. During all measurements, the temperature of the bulk electrolyte was maintained at 14 °C. Nyquist plots of the electrochemical impedance as a function of frequency for some values of the applied dc potential and for some angular velocities are shown in Figs. 5 and 6, respectively.

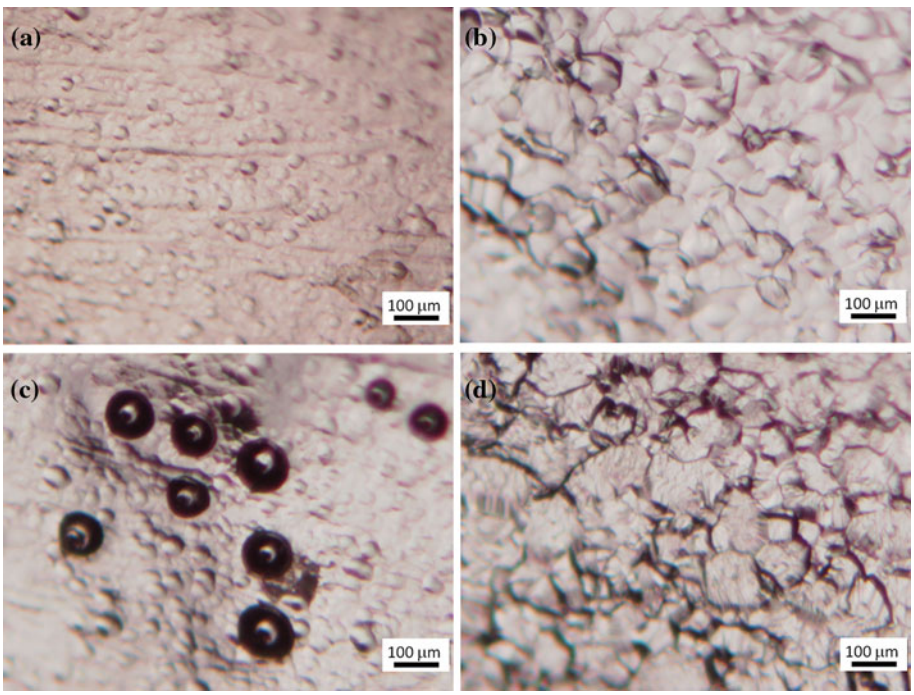

Fig. 3 Surface finish of flat Nb anode (**a**) and cathode (**b**) after polishing in the plateau region at J = 110 mA cm^{-2}, T_{bath} = 10 °C in the HF (49%):HNO_3 (70%):H_3PO_4 (85%) = 1:1:2 electrolyte. Pits were observed in some regions of the anode (**c**), while the surface finish of a Nb sample etched in the same solution is shown in (**d**). The size of each picture corresponds to a surface area of about 770 μm × 590 μm

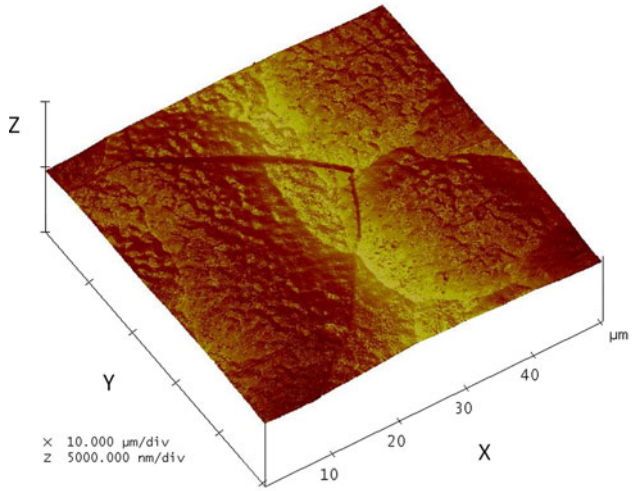

Fig. 4 Surface topography measured by AFM on a 50 µm × 50 µm area of the Nb anode polished in the plateau region at $J = 110$ mA cm^{-2}, $T_{bath} = 10$ °C in the HF (49%):HNO_3 (70%):H_3PO_4 (85%) = 1:1:2 electrolyte. The RMS roughness is 105 nm

From Fig. 5, multiple capacitive and inductive loops can be noticed over the covered frequency range of 1.6 Hz–200 kHz. The diameter of the high-frequency (~2.5–200 kHz) loop increases with increasing applied potential while it decreases with increasing rotation speed. In addition, the shape of this loop is that of a "depressed" semi-circle, indicating the presence of a non-ideal capacitance [11]. In the low-frequency range, the magnitude of the impedance increases as the potential is increased. The data taken with the RDE shown in Fig. 6 have larger scatter then those taken in static condition, most likely due to the large turbulence near the electrode because of the low-viscosity acid mixture used in these experiments. This may also explain why the data became extremely noisy at rotation speeds above 100 rpm. The electrolyte viscosities were measured with a Brookfield DV-II+PRO digital viscometer without stainless steel guard-leg. The dynamic viscosity was calibrated against viscosity standard. The variation of repeated viscosity measurements was about 1.5%. For BCP 1:1:2, the measured viscosity is 15.5 ± 0.4 cP at 10 °C and 14.1 ± 0.3 cP at 20 °C. For EP 1:10, the measured viscosity is 34.16 ± 0.15 cP at 10 °C and 26.34 ± 0.23 at 20 °C.

A plot of the reciprocal of the limiting current density as a function of the reciprocal of the square root of the angular velocity is shown in Fig. 7. The data follow a straight line with non-zero intercept, indicating that the current plateau in the polarization curve is not due to mass-transport limitation only but by a mixed mass-transport and kinetic control. The results from the EIS experiments will be discussed more in details in the next section.

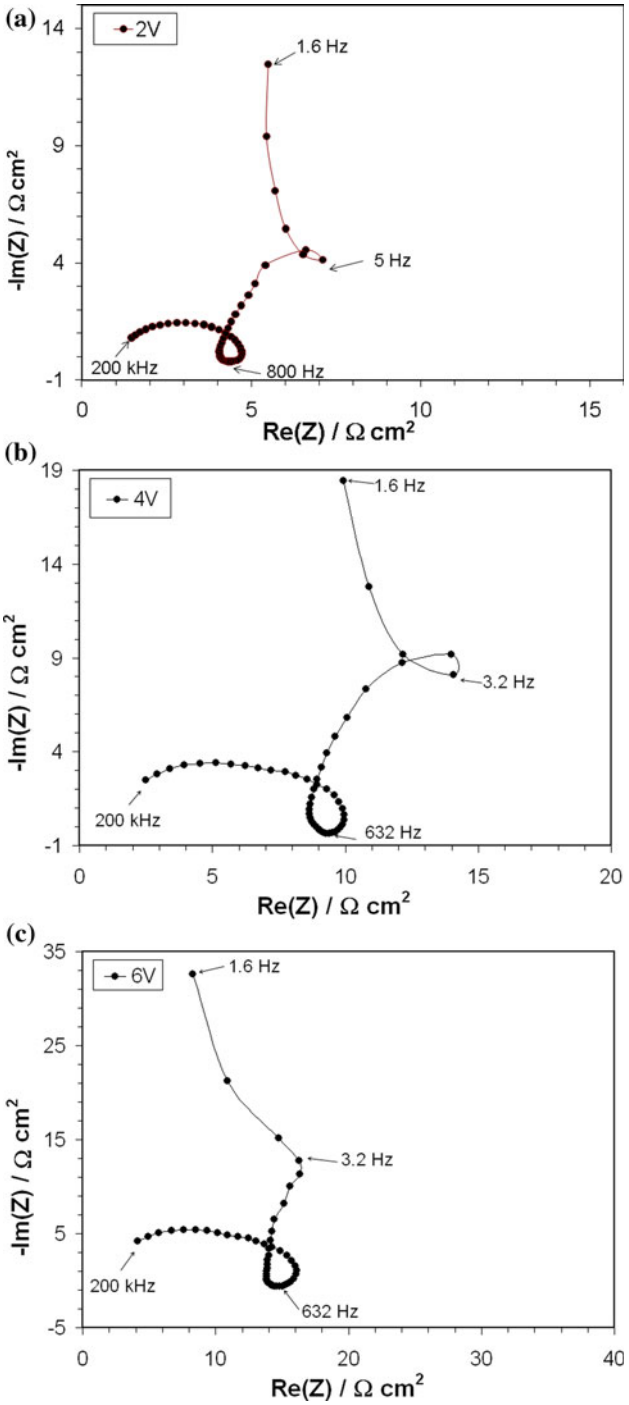

Fig. 5 Impedance diagrams for Nb disk electrode (no rotation) in HF (49%):HNO_3 (70%):H_3PO_4 (85%) = 1:1:2 electrolyte at 14 °C measured at different applied potentials in the current plateau region

4 Data analysis and discussion

The polarization curve of Nb in the same electrolyte used for BCP shows similarities with the polarization curve in HF:H_2SO_4 = 1:9 electrolyte, used for the EP of Nb: current oscillations occur within a certain range of the applied

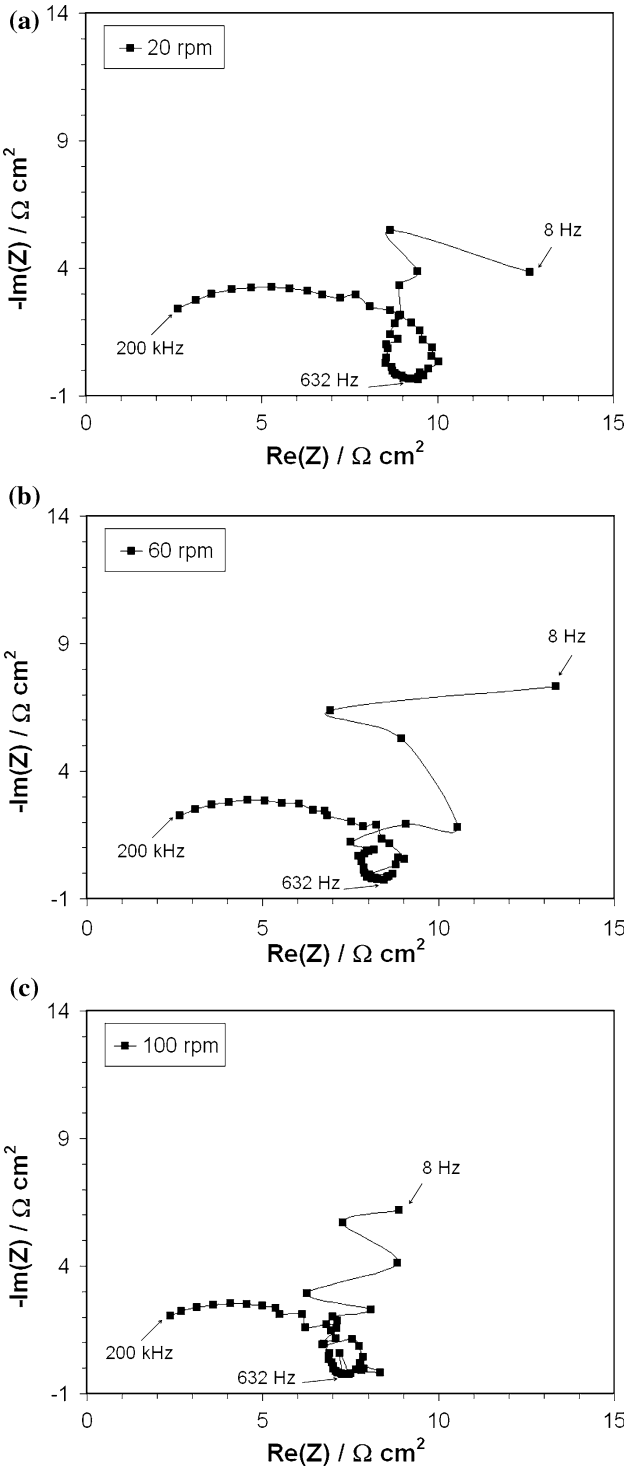

Fig. 6 Effect of rotation speed on the impedance diagram for Nb RDE in HF (49%):HNO_3 (70%):H_3PO_4 (85%) = 1:1:2 electrolyte at 14 °C and applied potential of 4 V versus MSE

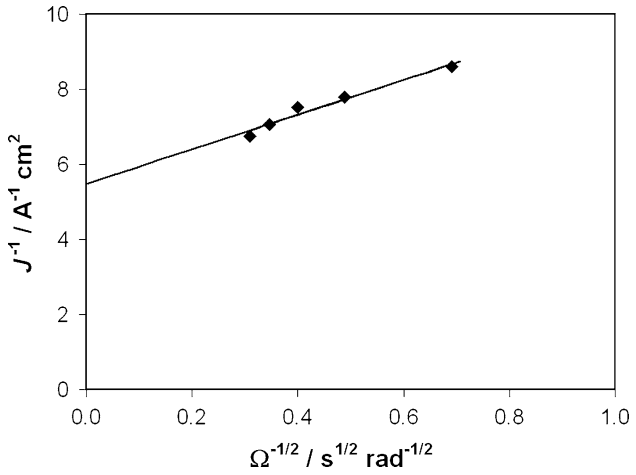

Fig. 7 Relation between the reciprocal of the limiting current density and the reciprocal of the square root of angular rotation speed determined for Nb in HF (49%):HNO_3 (70%):H_3PO_4 (85%) = 1:1:2 at 14 °C. The *solid line* is a linear fit of the data

anodic potential, followed by a plateau region at higher voltages [12]. The plateau region is commonly associated with a mechanism of limited mass transport of species such as the electrolyte anions and the cations and water molecules across a diffusion layer between Nb and the bulk solution. A recent investigation of EP on Nb revealed the presence of a compact salt film and that the diffusion-limited access of fluorine to the film limits the local reaction rate, causing the limited-current plateau [12]. The electrolyte used for EP of Nb has a mass fraction of sulfuric acid of about 90%. Sulfuric acid has a high viscosity and low dissociation constant (p$Ka = -3$), so that the oxidation reaction occurring at the anode can be written as [13]:

$$2Nb + 5H_2O \rightarrow Nb_2O_5 + 10H^+ + 10e^- \quad (1)$$

HNO_3 (70%) has the lowest dissociation constant among the acids used in the BCP mixture (p$Ka = -1.4$), so that the oxidation of Nb at the anode could be enforced by both NO_3^- anions and water:

$$8Nb + 10NO_3^- \rightarrow 4Nb_2O_5 + 10NO(g) + 10e^- \quad (2)$$

In all processes, Nb_2O_5 is then dissolved by HF as soluble niobium fluoride or oxyfluoride [13]. The phosphoric acid would have the same "buffer" role as during standard BCP. The etching rate and surface finish given by the cathodic polarization of Nb do not differ significantly from that of standard BCP, so the reaction most likely to occur there, besides BCP etching, is just the reduction of hydronium ions into hydrogen gas or the reduction of nitric acid into nitrogen oxide:

$$2H^+ + 2e^- \rightarrow H_2(g) \quad (3)$$

$$3H^+ + 3e^- + HNO_3 \rightarrow NO(g) + 2H_2O \quad (4)$$

The formation of gaseous nitrogen oxide among the reaction products in Eqs. 2 and 4 is supported by the evolution of a reddish-brown colored gas under the chemical flow hood: this is nitrogen dioxide, formed from the reaction of NO with the atmosphere.

Unlike during the standard EP process, active dissolution of the electrodes already occurs in the acid mixture considered in this study with zero applied potential. In addition the electrolyte used for this study has much lower viscosity compared to typical electrolytes used for EP. In general terms, the application of a potential to Nb electrodes immersed in BCP solution has the following effects:

- the cathode potential moves to more negative values, but the dissolution mechanism is mostly unchanged
- the anode potential moves to more positive values, i.e. to the passive region, and therefore Nb becomes coated by a thicker Nb_2O_5 layer and its dissolution occurs via the electrochemical etching of this oxide.

This general description of the process gives a qualitative explanation for the surface finish of the Nb electrodes shown in Fig. 3a and b. More information about the mechanisms governing the plateau region of the polarization curve can be obtained from the analysis of the EIS data. The presence of multiple loops in the Nyquist plot had been previously observed, for example, for the EP of Fe13Cr in a phosphoric acid-based electrolyte [14]. In that particular system the high-frequency loop is associated with a charge-transfer process and the lowest frequency loop is associated with the diffusion of a solvating acceptor species. The intermediate frequency loop is related to the formation of adsorbed ionic species which compete for available surface sites. The current plateau and the EP of Fe13Cr resulted from the transport limitation of the acceptor species from the bulk electrolyte to the surface of the dissolving metal [15].

Recent investigation of the Nb electrodissolution in acid fluoride medium [16] showed that the process occurring in the plateau region is consistent with the presence of an oxide film covering the metal and surface charges distributed on both sides of the oxide. The main features of this surface charge approach [10] can be summarized as follows: in the plateau region a barrier-like oxide film covers the metal surface and transport processes in its bulk become predominant in the response of the electrode system. Concentration profiles of metal and oxygen vacancies are such that negative and positive surface charges are present near the oxide/electrolyte and metal/oxide interfaces, respectively. These charges are at the origin of the inductive behavior observed in the impedance diagrams. Although evidence for non-negligible migration of niobium cations to the oxide-solution interface was found [17, 18], the model assumes that, in the steady state, film growth occurs mainly by transport of oxygen vacancies, under the effect of a constant electric field. This model is used to describe the medium-to-high frequency (20 Hz–200 kHz) impedance data, characterized by inductive and capacitive loops. The equivalent circuit from the surface

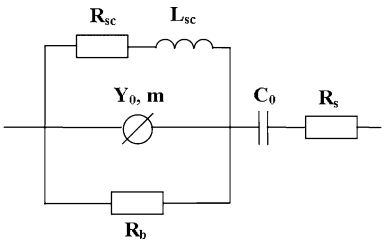

Fig. 8 Equivalent circuit used to describe the impedance diagrams in the 20 Hz–200 kHz range

charge approach model is shown in Fig. 8. A constant phase element of impedance $Z_{cpe} = 1/(j\omega)^m Y_0$ is used, instead of the ideal barrier film capacitance C_b used in Refs. [10, 16], in order to fit the "depressed" semicircle observed in the high-frequency impedance plots. The other parameters in the model are the resistance of vacancies migration, R_b, the elements R_{sc} and L_{sc} associated to the negative surface charge at the oxide/electrolyte interface, the faradaic pseudocapacitance C_0 and the electrolyte resistance R_s. According to the model, the physical parameters of the film growth are related to the experimental quantities determined in the impedance experiments (C_b, R_{sc}, L_{sc}, R_b and C_0) by the following relationships [10, 16]:

$$\frac{dC_b^{-1}}{dV} = \frac{1}{\varepsilon\varepsilon_0}\frac{dx}{dE} \tag{5}$$

$$\frac{d(R^* i)}{dV} = \left(\frac{zFa}{RT}\right)^{-1}\frac{dx}{dE} \tag{6}$$

$$C_0 = \frac{nF}{V_m \lambda}\frac{dx}{dE} \tag{7}$$

$$\frac{R_b}{R_{sc}} = \frac{\alpha}{1-\alpha} \tag{8}$$

$$\frac{L_{sc} j}{R_{sc}} = S^{-1} \tag{9}$$

where $R^* = [1/R_b + 1/R_{sc}]^{-1}$ is the effective resistance felt by the ionic transport at high frequency, a is the half-jump distance of the oxygen vacancies, α is the polarizability of the film/solution interface, S is the capture cross section for positive defects by the negative surface charge, and λ is the current efficiency for film formation. V_m is the molar volume of the oxide (Nb_2O_5), z is the electric charge of the mobile species ($z = 2$, since transport occurs mainly by oxygen vacancies), n is the number of elementary charges necessary to grow an oxide molecule ($n = 10$ for Nb_2O_5) and R, T, and F with their usual meaning. In addition, ε is the dielectric constant of the oxide and ε_0 is the permittivity of the free space. dx/dE is the so-called formation ratio, defined as the ratio between the increment in the oxide film thickness dx and the increment in the overall applied potential dE.

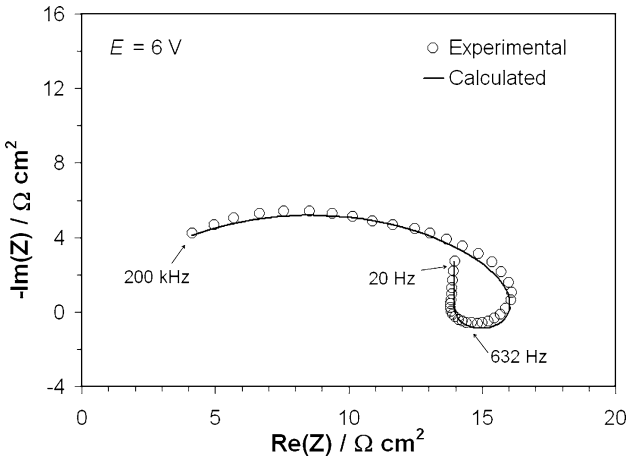

Fig. 9 Comparison of the experimental impedance diagram for Nb disk electrode (no rotation) at 6 V (relative to MSE) in HF (49%):HNO_3 (70%):H_3PO_4 (85%) = 1:1:2 electrolyte at 14 °C with the best fitted curve calculated according to the equivalent circuit of Fig. 7. The fit parameters are: $R_{sc} = 74\ \Omega\ cm^2$, $L_{sc} = 15.5$ mH cm^2, $R_b = 17\ \Omega\ cm^2$, $Y_0 = 0.32\ \mu S\ s^{m-1}\ cm^2$, $m = 0.692$, $C_0 = 2.9$ mF cm^{-2}

In order to determine the potential dependence of the circuit model parameters, a least-square fit of the experimental impedance data in the range 20 Hz–200 kHz was done with the impedance obtained from the circuit shown in Fig. 8, for several values of the applied potential. Figure 9 shows an example of such fit for $E = 6$ V compared with the experimental data. The solution resistance was kept constant at a value $R_s = 35\ m\Omega$ for all potentials. This value was obtained from $R_s = \rho/4R$ where $\rho = 35\ m\Omega$ cm is the resistivity of the solution measured earlier and $R = 0.25$ cm is the radius of the Nb disk electrode.

There exist different models to calculate the equivalent of the barrier capacitance, C_b, from the values of Y_0 and m obtained from the data fitting [19]. According to Brug et al. [20], the relationship between C_b and Y_0 is given by:

$$C_b = \left[Y_0 R_s^{(1-m)}\right]^{1/m} \tag{10}$$

which was found to give reliable results from data taken using an RDE setup [19]. An alternative relationship, given by Hsu and Mansfeld [21], is:

$$C_b = Y_0(\omega_m)^{m-1} \tag{11}$$

where ω_m is the angular frequency corresponding to the maximum of the imaginary part of the high-frequency impedance.

The average value of m obtained from the fits is about 0.694 ± 2%, independent of potential. Figure 10 shows a plot of the product R^*i and of C_b^{-1}, calculated from Eq. 10, as a function of the applied potential: the data are well fitted with a straight line, in agreement with the surface charge

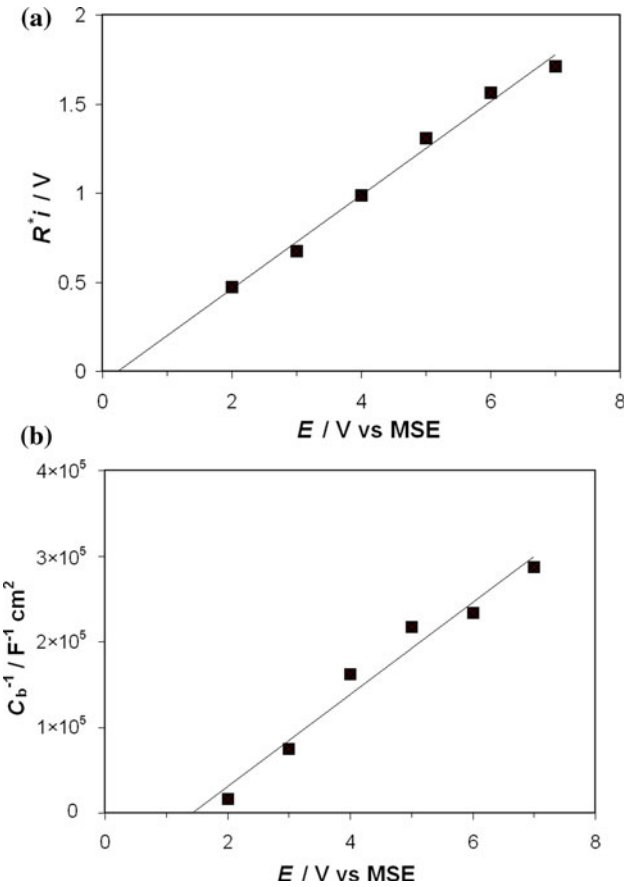

Fig. 10 Potential dependence of R^*i (**a**) and of C_b^{-1} (**b**) for a Nb disk electrode (no rotation) in HF (49%):HNO_3 (70%):H_3PO_4 (85%) = 1:1:2 electrolyte at 14 °C, fitted with a *straight line*

model. To determine the formation ratio dx/dE using Eq. 5 we need a value for the dielectric constant of the oxide: values of ε between 20 and 60 have been reported in the literature [22–24]. Assuming a value of $\varepsilon = 40$ and C_b calculated using Eq. 10, the value of the formation ratio was determined from Eq. 5 to be dx/d$E = 1.9 \pm 10\%$ nm V^{-1}. The value of a obtained from Eq. 6 is 0.1 ± 11% nm. We can then calculate the value of λ from Eq. 7 to be $\lambda = 0.97 \pm 13\%$. The value of α obtained from Eq. 8 is $\alpha = 0.19 \pm 10\%$ and the value of S obtained from Eq. 9 is 43 ± 16% $cm^2\ mC^{-1}$.

Considering the uncertainties in the value of the dielectric constant of Nb_2O_5 and in the determination of the equivalent barrier capacitance, the values of the physical parameters for the film growth obtained from our data are in fair agreement with the values reported in [16]. If Eq. 11 would have been used to calculate C_b, the formation ratio would have been higher than the value obtained using C_b calculated from Eq. 10, by about a factor of 25. As far as the mechanism causing the plateau in the polarization curve of Nb in HF:HNO_3:H_3PO_4 = 1:1:2 electrolyte, another important factor, besides vacancies migration

through the barrier oxide film as described in the surface charge approach, may be the transport limitation of the acceptor species. Because of the active dissolution of the Nb electrode already occurring at zero applied potential, large amounts of reactions products are formed on the anode surface and the ability of solvating species, such as water, to reach the surface could also contribute in limiting the reaction rate.

The fits of the impedance data in the 20 Hz–200 kHz range at an applied potential of 4 V (vs. MSE), as a function of the rotation speed, with the surface charge model indicate a linear decrease of R_b from about 10.7 Ω cm^2 at 0 rpm to about 8.5 Ω cm^2 at 100 rpm. The parameter S increases linearly from about 40 cm^2 mC^{-1} at 0 rpm to about 57 cm^2 mC^{-1} at 100 rpm. All the other parameters do not change with rotation speed. The following average values were obtained: $\alpha = 0.17 \pm 5\%$, $C_b = 8.27 \pm 20\%$ μF cm^{-2}, $m = 0.68 \pm 3\%$, and $C_0 = 3.39 \pm 16\%$ mF cm^{-2}.

Removal of just 40 μm from the Nb in the BCP 1:1:2 solution with anodic polarization applied, resulted in a significant reduction of the surface roughness, compared to what is typically obtained with the standard chemical etching. Although micro-smoothening of the Nb surface was achieved, the data from the RDE shown in Fig. 7 and the presence of pits, shown in Fig. 3c, suggest that mixed mass-transport and kinetic control mechanism occurs in the current plateau region of the polarization curve.

Pitting corrosion typically occurs due to a local breakdown of the oxide film. After this initiation, an anode forms where the film has broken, while the unbroken film acts as a cathode. The electrolyte inside the growing pit will further accelerate corrosion. Pitting, which has also observed on electropolished Nb samples and cavities, has been related to a degradation of cavity performance [25] and should therefore be avoided. In addition, hydrogen bubbles formed on the cathode surface from the process in Eq. 3 may also be responsible for pitting and potentially hydrogen loading of the niobium. Some degree of electrolyte agitation near the electrode, which is a standard practice during BCP etching but which was not applied in these experiments, and a good temperature control, for example, by flowing water on the back side of the electrode, should help reducing the probability of pitting on the surface.

5 Conclusions

Buffered electrochemical polishing of niobium in a mixture of phosphoric, nitric, and hydrofluoric acid has been explored for application to the surface preparation of Nb microwave resonators for particle accelerators. Applying a polarizing potential to Nb immersed in the same acid mixture commonly used for BCP was explored as an attempt to alter the oxide layer on the Nb surface and evaluate its influence on high-field RF losses. The electrochemical process was studied by measuring polarization curves and electrochemical impedance as a function of frequency, with and without electrolyte agitation. In the current plateau region, micro-polishing occurred, yielding smoother surfaces than by standard BCP process. As Nb cavities are typically subjected to several hundred microns of material removal by BCP after fabrication, a smoother surface could therefore be achieved by applying an anodic potential to the cavity, filled with the same electrolyte, removing about 40 μm as a final polishing step. The removal rate of the anodic polarized BCP is about a factor of two lower than standard BCP but about a factor of three faster than standard EP of Nb. Further optimization of process parameters such as temperature and acid flow rate is necessary, particularly to minimize pitting. The impedance data in the plateau region of the polarization curve can be interpreted in the frame of the surface charge approach developed by Bojinov [10] but with non-ideal barrier capacitance. The physical parameters of the model which give a good fit of the experimental data are fairly consistent with values obtained in an earlier study on the Nb electrodissolution in acid fluoride medium with fluorine concentration much lower than for the electrolyte used for this study.

Acknowledgments The authors would like to acknowledge O. Trofimova of the College of William and Mary for helping with the optical microscope and AFM measurements. This research was conducted at Thomas Jefferson National Accelerator Facility, operated by Jefferson Science Associates, LLC under U.S. DOE Contract No. DE-AC05-06OR23177. The U.S. Government retains a non-exclusive, paid-up, irrevocable, world-wide license to publish or reproduce this manuscript for U.S. Government purposes.

References

1. Kneisel P (2006) Nucl Instrum Methods A557:250
2. Lilje L (2001) PhD Thesis, University of Hamburg, Hamburg, Germany
3. Tian H (2008) PhD Thesis, The College of William & Mary, Williamsburg, Virginia, USA
4. Ciovati G (2006) Physica C 441:44
5. Saito K (2007) In: Proceedings of the 13th workshop on RF superconductivity, Beijing, China, TU202
6. Kneisel P, Myneni GR, Ciovati G, Sekutowicz J, Carneiro T (2007) AIP Conf Proc 927:84
7. Halbritter J, Kneisel P, Palmieri V, Pekeler M (2001) IEEE Trans Appl Supercond 11:1864
8. Halbritter J (1987) Appl Phys A 43:1
9. Ciovati G, Corcoran S G, Halbritter J (2007) In: Proceedings of the 13th workshop on RF superconductivity, Beijing, China, TUP17
10. Bojinov M (1997) J Solid State Electrochem 1:161

11. Barsoukov E, Ross Macdonald J (2005) Impedance spectroscopy: theory, experiment, and applications. Wiley-Interscience, New York
12. Tian H, Corcoran SG, Reece CE, Kelley MJ (2008) J Electrochem Soc 155:D563
13. Kneisel P (1980) In: Proceedings of the 1st workshop on RF superconductivity. Karlsruhe, Germany, p 27
14. Magaino S, Matlosz M, Landolt D (1993) J Electrochem Soc 140:1365
15. Matlosz M, Magaino S, Landolt D (1994) J Electrochem Soc 141:410
16. Cattarin S, Musiani M, Tribollet B (2002) J Electrochem Soc 149:B457
17. Rigo S, Siejka J (1974) Solid State Commun 15:259
18. Pringle JPS (1980) Electrochim Acta 25:1423
19. Orazem ME, Tribollet B (2008) Electrochemical impedance spectroscopy. Wiley-Interscience, New York
20. Brug GJ, Van Den Eeden ALG, Sluyters-Rehbach M, Sluyters JH (1984) J. Electroanal Chem 176:275
21. Hsu CH, Mansfeld F (2001) Corrosion 57:747
22. Robinson MLA, Roetschi H (1968) J Phys Chem Solids 29:1503
23. Gallego JM, Thomas CB (1983) Solid State Commun 47:419
24. Di Quarto F, Piazza S, Sunseri C (1990) Elecctrochim Acta 35:99
25. Zhao X, Ciovati G, Bieler TR (2010) Phys Rev ST Accel Beams 13:124701